# Dynamics of vortex lines in turbulent flows

Barak Galanti, Itamar Procaccia, and Daniel Segel
*Department of Chemical Physics, The Weizmann Institute of Science, Rehovot 76100, Israel*
(Received 9 May 1996; revised manuscript received 7 August 1996)

We examine the dynamic interplay between vorticity magnitude and vortex line geometry, and its relevance for curbing potential finite-time singularities in incompressible Navier-Stokes flows. We present direct numerical simulations of flows with various low and mid-range Reynolds numbers and different types of forcing. The central conclusion is that the vortex lines in regions of high vorticity tend to be straight and well aligned. Such an organization indicates the existence of a self-correcting mechanism that cancels the quadratic nonlinearity inherent in the vorticity equation. We consider several relevant effects, including the observation of straightening of vortex lines by stretching. [S1063-651X(96)11711-6]

PACS number(s): 47.27.−i

## I. INTRODUCTION

The aim of this paper is to examine the dynamics of vortex lines and vortex tubes in turbulent flows. Our motivation is that, on the one hand, numerical simulations [1–4] and experiments [5,6] indicate that even in highly complex turbulent flows the vortex lines in regions of intense vorticity appear to be quite straight on the scale of the entire system. Visualizations of the numerical data in these papers show the domination of the flow by a tangle of ''wormlike'' vortex tubes. We thus take, in this paper, the existence of such tubes as given, and indeed visualizations of vorticity isosets in the data presented here show a collection of very similar tubes. We note, on the other hand, the apparent lack of finite-time singularities in incompressible Navier-Stokes flows. It is tempting to propose that there exists a connection between the two phenomena. Indeed, it was proposed in [7] that such a connection is indicated by mathematical analysis. In this paper we proceed to examine the same issues on the basis of direct numerical simulations.

As is well known, the Navier-Stokes dynamics of the vorticity contains a term that may lead to a finite-time singularity. To see this we start from the Navier-Stokes (NS) equations for the velocity field $\mathbf{u}(\mathbf{x},t)$ of an incompressible fluid

$$D_t\mathbf{u}\equiv\frac{\partial\mathbf{u}}{\partial t}+(\mathbf{u}\cdot\boldsymbol{\nabla})\mathbf{u}=-\boldsymbol{\nabla}p+\nu\nabla^2\mathbf{u}+\mathbf{f}, \tag{1}$$

$$\boldsymbol{\nabla}\cdot\mathbf{u}=0, \tag{2}$$

where $p(\mathbf{x},t)$ is the pressure, $\mathbf{f}(\mathbf{x},t)$ is the external driving, and $\nu$ is the kinematic viscosity. Defining the vorticity $\boldsymbol{\omega}$ as $\boldsymbol{\omega}\equiv\boldsymbol{\nabla}\times\mathbf{u}$, we find the vorticity equation (disregarding the forcing)

$$D_t\boldsymbol{\omega}\equiv\frac{\partial\boldsymbol{\omega}}{\partial t}+(\mathbf{u}\cdot\boldsymbol{\nabla})\boldsymbol{\omega}=(\boldsymbol{\omega}\cdot\boldsymbol{\nabla})\mathbf{u}+\nu\nabla^2\boldsymbol{\omega}. \tag{3}$$

The term that can lead to singular growth is the first term on the right-hand side of this equation. Since $\boldsymbol{\omega}$ is the antisymmetric part of $\boldsymbol{\nabla}\mathbf{u}$ this term is potentially quadratic and may lead to finite-time singularities. This can be seen more explicitly in the equation for the vorticity magnitude

$$\frac{\partial\omega}{\partial t}+(\mathbf{u}\cdot\boldsymbol{\nabla})\omega-\nu\nabla^2\omega=(\alpha-\nu|\boldsymbol{\nabla}\boldsymbol{\xi}|^2)\omega. \tag{4}$$

In this equation $\boldsymbol{\xi}=\boldsymbol{\omega}/\omega$ and

$$\alpha=\boldsymbol{\xi}\cdot(\boldsymbol{\xi}\cdot\boldsymbol{\nabla})\mathbf{u}. \tag{5}$$

One can express the ''stretching rate'' $\alpha$ in terms of the vorticity by using the Biot-Savart inversion of the curl operator, giving us the expression [8]

$$\alpha(\mathbf{x})=\frac{3}{4\pi}\int(\hat{\mathbf{y}}\cdot\boldsymbol{\xi})\{\hat{\mathbf{y}}\cdot[\boldsymbol{\omega}(\mathbf{x}+\mathbf{y})\times\boldsymbol{\xi}(\mathbf{x})]\}\frac{d\mathbf{y}}{|\mathbf{y}|^3}. \tag{6}$$

We see that this integral over the vorticity includes a contribution from the vorticity at the point $\mathbf{x}$. If the vorticity increases at a point the stretching rate at that point increases and the possibility of a finite-time singularity is created. Indeed, numerical simulations of highly symmetric flows by Kerr [9] and Boratav and Pelz [10] indicate that the Euler (inviscid) incompressible equations can reach a finite-time singularity in certain specific situations. Such evidence of blowups has not been observed in viscid flow.

It is entirely possible that in physical systems the potential singularity is avoided by mechanisms that are not contained in the incompressible equations. For example, an abnormal local increase in vorticity may be carried away by sound modes that are dispersed over a long distance. Yet one recognizes that no finite-time singularity has ever been seen in simulations of incompressible fluids, and it is thus interesting to ask whether those fluids exhibit mechanisms to avoid such singularities as well. We thus seek mechanisms to curb blowups that stem from the geometry of the vorticity field. In particular we revisit in this paper ideas presented recently [7] that connect the dynamics of vortex lines with such mechanisms. Vortex lines are those lines that are everywhere tangent to $\boldsymbol{\omega}$. It can be seen directly from (5) that if the vortex field is locally aligned and straight, the local contribution to $\alpha$ vanishes and with it the possibility of finite-time singularity. The main theoretical idea proposed in [7] is that in those regions undergoing strong stretching, there is also a mechanism for local straightening of the vortex lines. This paper attempts to examine this idea further with the help of direct

 

numerical simulations. Furthermore, we examine in general the statistics of geometric properties such as the curvature and torsion as characteristics of the flow field.

The structure of the paper is as follows. In Sec. II we discuss the relevant characteristics of vortex lines: their curvature, torsion, and alignment with respect to neighboring lines. In Sec. III we present our numerical methods of simulation and analysis. Section IV deals with results that pertain to low Reynolds number flows. We stress in this section the importance of the structure of the vorticity field near zeros of the field and the independence of the strength of curvature from that of the energy contained in small scale modes. In Sec. V, which is the central section of this paper, high Reynolds flows are considered. The main conclusions from the simulations are that indeed in high vorticity regions vortex lines are relatively straight and aligned and that there are strong correlations between the magnitude of stretching and straightness of the vorticity field. We feel that these numerical results on the whole strengthen the possible connection between the dynamics of vortex lines and the control of blowups in the incompressible Navier-Stokes equations.

## II. GEOMETRY OF VORTEX LINES

### A. Frenet frame

In this study we will consider three geometrical quantities characterizing the vortex lines: their *curvature*, *misalignment* and *torsion*. Each is a local quantity, defined in terms of the vorticity direction field $\boldsymbol{\xi}$ [11–13].

The $|\nabla\boldsymbol{\xi}|$ measures the departure of the vortex lines from complete straightness and alignment; it is the inverse of a length scale. The curvature is defined as [14]

$$c=\frac{1}{R}\equiv|(\boldsymbol{\xi}\cdot\nabla)\boldsymbol{\xi}| \tag{7}$$

and is the inverse of the radius of curvature $R$ of the vortex line.

One can define at each point in a vector field a local orthogonal frame called the *Frenet frame* [14], defined in terms of three orthogonal unit vectors, the first in the vector field direction $\boldsymbol{\xi}$, the second in the direction of the curvature $\mathbf{n}$ of the vortex line $(\boldsymbol{\xi}\cdot\nabla)\boldsymbol{\xi}=c\mathbf{n}$ and the completing binormal $\mathbf{b}$. The torsion $T$, also with units of an inverse length scale, can be written in closed form as

$$T=|(\boldsymbol{\xi}\cdot\nabla)\mathbf{b}| \tag{8}$$

and represents the turning of the binormal as one goes along the filament; in other words, it represents the local deviation of the vortex line from a plane, just as the curvature represents the local deviation of the vortex line from straightness. Curved lines have $c\neq 0$, twisted lines have $T\neq 0$.

The total $|\nabla\boldsymbol{\xi}|$ can be seen as the vector sum of the curvature and the lack of alignment between the vortex lines and the neighboring lines in the normal and binormal directions

$$|\nabla\boldsymbol{\xi}|^2=c^2+|(\mathbf{n}\cdot\nabla)\boldsymbol{\xi}|^2+|(\mathbf{b}\cdot\nabla)\boldsymbol{\xi}|^2. \tag{9}$$

We can thus define the misalignment by

$$N^2=|\nabla\boldsymbol{\xi}|^2-c^2=|(\mathbf{n}\cdot\nabla)\boldsymbol{\xi}|^2+|(\mathbf{b}\cdot\nabla)\boldsymbol{\xi}|^2. \tag{10}$$

$N$ expresses the lack of alignment of a vortex line relative to its neighbors, through local twisting or divergence.

### B. Line geometry and dynamics

One can distinguish between viscid and inviscid effects in vorticity dynamics, corresponding to the second and first terms of Eq. (3) respectively. In the context of inviscid dynamics one can also distinguish between locally induced and nonlocally induced vorticity growth, corresponding, respectively, to the close and distant integration ranges in Eq. (6).

Different forms of vortex line distortion can contribute to the locally induced vorticity growth. The analysis of [7] considered well-aligned tubes, defined as those for which the curvature dominates the total distortion $|\nabla\boldsymbol{\xi}|$. The ''local'' rate of stretching $\alpha_{\mathrm{loc}}$ was calculated. By the ''local'' contribution to $\alpha(\mathbf{x})$ we mean the integral of Eq. (6) taken only over a small ball around $\mathbf{x}$. This contribution was found to be proportional to the vorticity and the curvature

$$\alpha_{\mathrm{loc}}\sim\omega c. \tag{11}$$

This would seem to create a quadratic nonlinearity in Eq. (3), leading to a finite-time singularity; a similar effect can arise in the local growth rate for any geometry.

Reference [7] then uses the Navier-Stokes equation, Eq. (2) to derive an equation for the inviscid evolution of the curvature

$$D_tC=-\alpha c-TS_b+(\boldsymbol{\xi}\cdot\nabla)S_n, \tag{12}$$

where $S_b$ and $S_n$ are two strain tensor components

$$S_b\equiv\mathbf{b}\cdot S\cdot\boldsymbol{\xi},\quad S_n\equiv\mathbf{n}\cdot S\cdot\boldsymbol{\xi}. \tag{13}$$

Reference [7] suggested that since no particular correlations are expected between the terms on the right-hand side, in regions of rapid growth of vorticity (so that $\alpha$ is high) the first term will be dominant and will straighten the vortex at just the same rate that the vorticity grows. Thus in Eq. (12) the growth in the vorticity will be canceled by the growth in the radius of curvature and the size of the local contribution to $\alpha$ will saturate; this will turn the potential finite-time singularity in Eq. (3) into exponential growth.

Reference [7] also considers the effect of viscosity on the vortex lines. It was shown that there exist viscid effects that enhance alignment and straightening of vortex lines, particularly in regions of strong vorticity magnitude.

Thus Ref. [7] considers two effects that can influence the connection between vorticity magnitude and curvature: the straightening of vortex lines by stretching and by viscid smoothing, both causing curvature to decrease with increasing vorticity. The first should be strong in regions of strong enough vorticity to ensure that a large $\alpha$ has been operating for some time, the second in medium-strength vorticity regions where diffusion has had a chance to be effective.

However, we here note that two other effects influencing the connection between vorticity magnitude and curvature can have a role. A third effect has the same tendency for low vorticity magnitudes. Look at the vicinity of a zero point of

the vorticity. Use coordinates based at a zero point and with axes in the eigendirections of the vorticity gradient tensor. Near the zero the vorticity is

$$\omega_x = \alpha x, \quad \omega_y = \pm \beta y, \quad \omega_z = -\gamma z \tag{14}$$

(from incompressibility $\alpha \pm \beta - \gamma = 0$). One can then verify that both the curvature and the misalignment diverge when approaching the zero point. Given this structure, in a monotonic neighborhood around a zero point both the curvature and the misalignment will decrease with increasing vorticity. The effect should also persist in a smooth neighborhood of time after the disappearance of such a zero point. A further consequence of the incompressibility of vorticity $\nabla \cdot \boldsymbol{\omega} = 0$ is that

$$\nabla \cdot \boldsymbol{\xi} = -\frac{(\boldsymbol{\xi} \cdot \nabla)\omega}{\omega}. \tag{15}$$

This quantifies a natural conclusion from Kelvin's law: it implies that if going along a vortex line the vorticity goes to zero, $\nabla \cdot \boldsymbol{\xi}$, and therefore the total distortion $|\nabla \boldsymbol{\xi}|$, diverges. It also shows that if along a vortex line there is a polynomial rise in the magnitude of vorticity, it is necessarily accompanied by a drop in the divergence $\nabla \cdot \boldsymbol{\xi}$ in the vorticity direction. This effect should be strong near zero-vorticity points and in regions of polynomial growth. Divergence is a part of the total misalignment and entails curvature generically since a swelling vortex tube has curved vortex lines. This means that a *blowup* of divergence implies a blowup of misalignment and curvature. *Correlations* between divergence and vorticity can also affect the latter three quantities, although such a link is not strictly necessary.

Finally, as it is clear from our former discussion, curvature can induce local stretching. If the local induction could be consistently dominant, this fourth effect would create high vorticity in highly curved regions. In view of the discussion in [7], this would happen if the other strain components happen to keep the curvature high despite stretching. This effect should be strong in regions of high curvature and high vorticity.

To summarize, the first three effects act to create a negative correlation between curvature and vorticity, while the fourth acts to create a positive correlation; the first effect should hold, as far as we can see, for curvature only, while the last three hold equally for curvature and misalignment. The study of the connection between curvature or misalignment and vorticity magnitude will take a central role in our study.

We finally discuss torsion. Of the above four effects, only the third does not hold for torsion since torsion does not necessarily diverge near a zero point. A dynamic equation for the torsion is derived in [7] in the same way as for the curvature; the result is

$$D_t T = -\alpha T + c S_b + (\boldsymbol{\xi} \cdot \nabla)\left[\frac{T}{c} S_n + \frac{1}{c}(\boldsymbol{\xi} \cdot \nabla) S_b\right], \tag{16}$$

so one would expect stretching to reduce torsion in the same way that it reduces curvature. In [7] it is shown that diffusion too reduces the torsion of vortex lines.

## III. METHODS

### A. Simulation

The data analyzed comes from our direct numerical simulations of isotropic homogenous turbulence in a periodic box. A pseudospectral method was used. Dealiasing was performed by setting all $\tilde{\mathbf{u}}(\mathbf{k})$ with $k > \frac{2}{3} k_{\max}$ to zero before transforming the $\tilde{\mathbf{u}}(\mathbf{k})$ to real space in order to perform a product. (One might mention that no significant differences between runs with and without aliasing were observed.) The runs were performed on a Cray C94 supercomputer at the Cray Research Center, the Cray J916 at the Weizmann Institute and the Cray J932 at Israel's Inter University Computer Center.

For most of the runs the forcing used was the Arnold-Beltrami-Childress (ABC) force [15], which is defined in terms of the ABC velocity field **U**, whose components are

$$\begin{aligned} U_x &= A\sin(k_0 z) + C\cos(k_0 y), \\ U_y &= B\sin(k_0 x) + A\cos(k_0 z), \\ U_z &= C\sin(k_0 y) + B\cos(k_0 x). \end{aligned} \tag{17}$$

This flow is a solution of the Euler equations (i.e., the NS equations with $\nu = 0$ and no forcing) and a solution of the NS equations with forcing given by the ABC *force* $\mathbf{f} = \nu k_0^2 \mathbf{U}$. The reason for using this forcing was the existence of detailed studies of this flow at low Reynolds numbers [16,17] and the ability of the flow to excite turbulence rapidly due to its chaotic nature.

In our runs we used the parameters $A = B = C = 1$ and $k_0 = 1$. The ABC solution for this forcing loses its stability at $\mathrm{Re} = 13.05$ [16] (we here use the definition $\mathrm{Re} = 1/\nu$). Galloway and Frisch [16] and later Podvigina and Pouquet [17] have studied the stability of this flow for a range of Reynolds numbers and found that it undergoes a series of bifurcations and reaches a temporally chaotic state for $\mathrm{Re} > 23$.

Some runs were also performed using a random forcing in order to see if some of the effects we observe might result from the particular form of the ABC force. The random force used, in particular, has chiral symmetry and is much less coherent in time than the ABC force. We forced all the modes with $|\mathbf{k}| < 2.5$, i.e., the modes $(\pm 1,0,0)$, $(\pm 1,\pm 1,0)$, $(\pm 1,\pm 1,\pm 1)$, $(\pm 2,0,0)$, and $(\pm 2,\pm 1,0)$ and their permutations. The forcing was of white noise form, i.e. the real and imaginary parts of each of the complex Fourier components of each mode were chosen as two independent random numbers distributed uniformly between 1 and $-1$, with no correlations in space or time.

A number of runs at various integral-scale Reynolds numbers were performed. The parameters of the runs are summarized in Table I.

### B. Analytic routines

In principle the calculation of the geometrical quantities could be done using the definitions [see Eqs. (7) and (8)] given in the Introduction. However, this makes the calculation in Fourier space of derivatives impossible; these quantities, which involve derivatives of the vorticity direction field $\boldsymbol{\xi}$, are singular at those points where $\boldsymbol{\xi}$ is undefined, i.e.,

TABLE I. Parameters of the various numerical runs.

| Run | Forcing | Mesh | Re | $\mathrm{Re}_\lambda$ | $L$ |
|---|---|---|---|---|---|
| ABC-20 | ABC | $32^3$ | 20 | 43 | |
| ABC-30 | ABC | $32^3$ | 30 | 56 | |
| ABC-100 | ABC | $64^3$ | 100 | 43 | 2.1 |
| ABC-500 | ABC | $128^3$ | 500 | 56 | 1.8 |
| ABC-1000 | ABC | $128^3$ | 1000 | 68 | 1.75 |
| ABC-1500 | ABC | $128^3$ | 1500 | 76 | 1.7 |
| ABC-2200 | ABC | $192^3$ | 2200 | 93 | 1.75 |
| R-300 | random | $64^3$ | 300 | 60 | 1.7 |
| R-1500 | random | $128^3$ | 1500 | 80 | 2.0 |

where $\omega=0$. Because of this problem, formulas were used expressing all quantities in terms of derivatives of the vorticity vector, which is regular and differentiable everywhere. The formulas for calculation of the curvature, total distortion, and torsion are given in the Appendix.

The code for the calculations was checked on two kinds of simple flows. For very simple flows the geometric calculations can be done analytically. Specifically, expressions were found for the curvature in the Roberts flow

$$u_x^R=\sin(x)\cos(y),$$
$$u_y^R=-\cos(x)\sin(y),$$
$$u_z^R=\sqrt{2}\sin(x)\sin(y), \tag{18}$$

and for the Roberts flow modified by a uniform flow $\boldsymbol{\omega}=\mathbf{u}^R+(a,0,0)$. In addition, we calculated the curvature, misalignment and torsion (equal to zero) in the flow

$$\omega_x=a+\sin(x),$$
$$\omega_y=a,$$
$$\omega_z=a, \tag{19}$$

with $a$ an arbitrary constant. Comparisons with the numerical results of our code gave excellent results, maximal errors not exceeding machine precision. For more complex flows finding an analytic expression for the geometric quantities is prohibitively difficult, but derivatives of the velocity field can be performed analytically rather easily. We can then use these expressions for the derivatives to calculate geometric quantities by performing the remaining algebra numerically. Calculations of this type were performed for the ABC flow with $A=B=C=1$ and for the Roberts flow for curvature, misalignment, and torsion. Comparisons with our code's results were again excellent, with maximal errors reaching $10^{-10}$.

### C. Statistical analysis

The code used produced directly as output statistical analyses of the quantities studied, in the form of probability distribution functions (PDFs) and what we call weighted distribution functions (WDFs). The PDF of a quantity $x$, such as curvature, is calculated by dividing a given range of possible values of $x$ into a number of discrete boxes, counting the number of points whose value of $x$ falls within each box, then normalizing by the total number of points. A WDF is designed to find the dependence of a quantity $x$ (say, the curvature) on a quantity $y$ (say, vorticity) on average. To do this, we divide a range of values of $y$ into a number of boxes and find the number of points whose value of $y$ falls in each box and the sum of the values of $x$ of these points; we then divide this sum by this number of points to find the average value of $x$ in each box. Such statistical functions were recorded at regular intervals, frequently enough to follow the main developments of the dynamics and to allow good statistics. The data sets consists of at least 40 outputs for every run and reaching up to several hundred outputs for the low Reynolds runs.

We will now make a few remarks about PDFs in general. We begin with a formula for the PDF of a scalar quantity in space, assuming that the dependence of this quantity on space is given.

Given a function $T(\mathbf{x})$ defined in some volume $V$, the PDF $P(T)$ is given by

$$P(T)=\frac{1}{V}\frac{dV(T)}{dT}, \tag{20}$$

where $V(T)$ is the volume of points with $T(\mathbf{x})\leqslant T$. That is, for small $\Delta T$,

$$P(T)\Delta T=\frac{1}{V}[V(T+\Delta T)-V(T)]. \tag{21}$$

This is just the formula that we use for our numerical calculations. If we use a measure $dx_1dx_2$ on the surface $\partial V(T)$ of $V(T)$ and $dx_3$ for the integration normal to the surface $\partial V(T)$, the normal direction depending on the position on the surface $(x_1,x_2)$, then as $\Delta T\to 0$ we have

$$P(T)=\frac{1}{V}\int_{\partial V(T)}dx_1dx_2\frac{1}{|\boldsymbol{\nabla} T(x_1,x_2)|}. \tag{22}$$

In discretized space the version of this formula is

$$P(T)=\frac{1}{n}\sum_{T(\mathbf{x})=T}\frac{1}{|\boldsymbol{\nabla} T(\mathbf{x})|}, \tag{23}$$

where the sum is over all points in the volume considered that have the specified value of $T$ and $n$ is the total number of points in the volume. While this formula is impractical for

use in numerical calculations, it allows us to conclude that the value of the PDF for a certain value is determined not only by the number of points that have that value but also by the form (and in particular the steepness) of the function at the relevant points.

In particular, the PDF diverges at extremal points of the function, unless the two-dimensional measure of the level set of the value concerned is zero. The PDF can also diverge if the level set's two-dimensional measure diverges, i.e., if the set's dimension becomes larger than 2. The PDF vanishes at points where the gradient of the function diverges and at points where the level set dimension drops below 2.

## IV. LOW REYNOLDS FLOW AND GEOMETRY

In this section we present our observations of low Reynolds flows, i.e., those with integral-scale Reynolds number of Re=20 and 30, together with similar geometric analyses of two ABC flows. Our main objective is to see how we can connect analytic understanding and numerical results of the geometry of flows simpler than fully turbulent flows. We first observe the Re=20 flow and see that it spends most of the time near one of three ABC attractor flows. We next analyze the geometry first of the ABC attractor flows, then of the Re=20 flow. Finally we see how the flow changes as the Reynolds number begins to rise.

### A. Nature of the Re=20 flow

We first consider the Re=20 runs. As noted by Podvigina and Pouquet in their study [17] of low-Reynolds ABC-forced flow, at this Re the initial ABC flow (that with $A=B=C=1$) is unstable, and after a period of exponential growth and saturation of the small scales the flow alternates between three attracting metastable flows in phase space. In these flows the large-scale modes are close to those of ABC flows with $k_0=1$ and $(A,B,C)=(0.48,0.48,1.34)$, (0.48,1.34,0.48), and (1.34,0.48,0.48), respectively. Thus, through the period in which the flow is near each one of these metastable flows a different ABC mode becomes energetically dominant. Podvigina and Pouquet call these ABC flows the $\mathcal{A}_2$ flows and call the $A=B=C=1$ flow the $\mathcal{A}_1$ flow. The full metastable flow is an $\mathcal{A}_2$ flow distorted by small-scale components created by the excess of incoming energy over the energy lost by the dissipation of the ABC modes.

We can see this behavior in our run; as in the work of Podvigina and Pouquet, the ABC modes $\mathbf{k}=(1,0,0)$, (0,1,0), and (0,0,1) alternate in dominating the flow except for short transients. In our study too the small-scale modes are sizable particularly in the short periods of transition between $\mathcal{A}_2$ states. Our results for the chaotic behavior of the ABC modes and energy shells correspond closely to that presented by Podvigina and Pouquet.

The similarity of the turbulent flow during the metastable periods to stationary flows with a simple analytic form makes the Re=20 flow a good place to start a numerical examination of the geometry of vortex lines. In Fig. 1 we show the PDFs and WDFs of dependence on vorticity of the curvature, $|\nabla\boldsymbol{\xi}|$, and torsion in the $\mathcal{A}_1$ and $\mathcal{A}_2$ flows and at times of metastable and transitional Re=20 flow.

### B. Geometry of the attractor flows

We here consider and understand the $\mathcal{A}_1$ and $\mathcal{A}_2$ (ABC) flows and see how we can understand analytically the main features of the statistics of curvature and $|\nabla\boldsymbol{\xi}|$ in these flows. We will use the description of the qualitative nature of the $\mathcal{A}_1$ flow found in the study of Childress and Soward [18]. They showed that the flow contains a set of stagnation points connected by a network of straight streamlines. The flow around these stagnation points is characterized by hyperbolic behavior of two types. Since the sum of the eigenvalues of the strain tensor must be zero from incompressibility, not all of the eigenvalues can be either positive or negative, implying hyperbolicity near the stagnation points. In points with two positive eigenvalues of the strain tensor, the flow comes in towards the stagnation point in a narrow jet around the straight streamline and then fans out into a unstable surface on which the stagnation point lies. In points with one positive eigenvalue of the strain tensor the flow comes into the stagnation point from all directions on a stable surface, exiting the vicinity of the stagnation point in a narrow jet around the straight streamline. The points of maximal vorticity along a streamline lie between stagnation points of these two types, where the flow from a point with one positive eigenvalue reaches maximal convergence before starting to diverge again towards a point with two positive eigenvalues. The points with the highest vorticity ($\omega=6$) in the $\mathcal{A}_1$ flow lie on the streamlines parallel to the $x=y=z$ direction, called the primary streamlines by Childress and Soward.

We have made a similar qualitative analysis of the geometry of the $\mathcal{A}_2$ flow. This is simpler than that of the $\mathcal{A}_1$ flow, having a lower symmetry of structure. If we analyze, e.g., the $\mathcal{A}_2$ case with $B=C$, we can see that here too a set of straight streamlines exist. These lines on the $x$-$y$ planes are given by $z=\pi/4+m\pi/2$, as seen in Fig. 2. The flow along each straight streamline is constant in direction; there are no stagnation points in this flow. The direction of the flow in these streamlines rotates by $\pi/2$ from one plane to another, so that the direction of flow on a plane is opposite that on its next-nearest neighbor. The parallel streamlines on each plane are $\sqrt{2}\pi$ apart. The flow near the straight streamline has the shape of a swirling vortex tube (that is, the streamlines are twisted) diverging around the points $\mathbf{x}_{\min}$ of minimal vorticity and converging around the points of maximal vorticity $\mathbf{x}_{\max}$.

As shown by Dombre *et al.* [19], between the straight streamlines in all ABC flows the flow is dominated by a system of tubelike regions in which the flow is predominantly in the $x$ direction, in the $y$ direction, and in the $z$ direction, although the tubes do also twist appreciably. We will, however, refer less to these structures in our following analysis.

From these structures follow the dependences of curvature and $|\nabla\boldsymbol{\xi}|$ on vorticity magnitude seen in Figs. 1(b) and 1(d). The $|\nabla\boldsymbol{\xi}|$ when traveling along a primary streamline in the $\mathcal{A}_1$ flow goes from a minimal value at the point of maximal convergence and vorticity to a divergence towards the stagnation point. One can verify from Childress and Soward's expansion of the flow field near the primary streamline that the $|\nabla\boldsymbol{\xi}|$ at the $\mathbf{x}_{\max}$ point, where the divergence and curvature are zero, is minimal despite the fact that

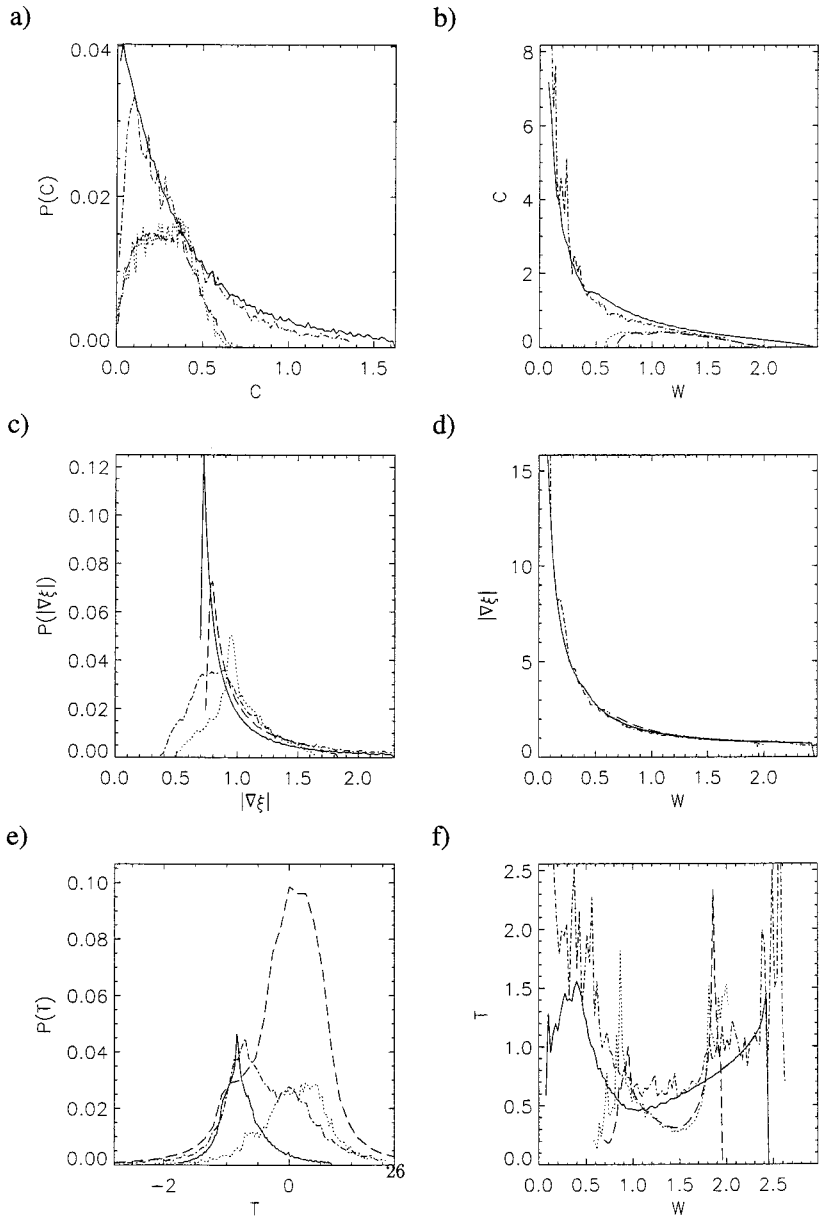


FIG. 1. Low Reynolds geometry: PDFs and dependence (WDF) of curvature on vorticity $\omega$ [(a) and (b) respectively], total distortion [(c) and (d)], and torsion [(e) and (f)]. Solid line, $\mathcal{A}_1$ flow, dashed line, $\mathcal{A}_2$ flow, dotted line Re=20 metastable flow; dash-dotted line, during a Re=20 small-scale burst. Note the similarity between the small-scale burst and $\mathcal{A}_1$ and between metastable and $\mathcal{A}_2$ flows.

the swirl of the flow around the streamline is strongest there. The rest of the flow follows this pattern and we get the decline of $|\nabla\boldsymbol{\xi}|$ with vorticity seen in Fig. 1(d). This dependence in the $\mathcal{A}_2$ flow is remarkably similar to that in the $\mathcal{A}_1$ flow, within the narrower range of vorticity magnitudes available in the $\mathcal{A}_2$ flow. In fact, it seems that if we take the $\mathcal{A}_1$ flow around the streamlines, as it goes from zero to maximal vorticity, and truncate the bundle at those vorticities corresponding to that range of vorticity magnitudes available in the $\mathcal{A}_2$ flow, we will get something very similar to the bundle around the streamlines in the $\mathcal{A}_2$ flow. Naturally, at the top and bottom of this range of vorticities some adjustment must be made, as can be seen in Fig. 1(d).

Further understanding of the $|\nabla\boldsymbol{\xi}(w)|$ dependence can be gathered from the equation

$$|\nabla\boldsymbol{\xi}|^2=\frac{1}{\omega^2}|\nabla\boldsymbol{\omega}|^2-\frac{1}{4\omega^4}|\nabla\omega^2|^2. \tag{24}$$

On the other hand, one can verify that for any ABC flow $|\nabla\boldsymbol{\omega}|^2=A^2+B^2+C^2$ (for $k_0=1$), which is simply a constant (in our numerics taken to be equal to 3). Thus, for any ABC flow

$$|\nabla\boldsymbol{\xi}|^2=\frac{A^2+B^2+C^2}{\omega^2}-\frac{1}{4\omega^4}|\nabla\omega^2|^2. \tag{25}$$

This immediately gives for extremal points $\mathbf{x}_{\rm ex}$ of vorticity $\omega=\omega_{\rm ex}$, where $\omega_{\rm ex}\neq 0$, the value

$$|\nabla\boldsymbol{\xi}(\mathbf{x}_{\rm ex})|=\frac{\sqrt{A^2+B^2+C^2}}{\omega_{\rm ex}}. \tag{26}$$

The robust dependence of $|\nabla\boldsymbol{\xi}|$ on $w$ might suggest that one could derive an exact relation between the two, at least for ABC flows. In fact, expansion near the $\mathbf{x}_{\rm min}$ points of the $\mathcal{A}_1$ flow shows that vorticity and $|\nabla\omega^2|$ are not one-to-one functions, as the isosurfaces of one quantity is a small dis-

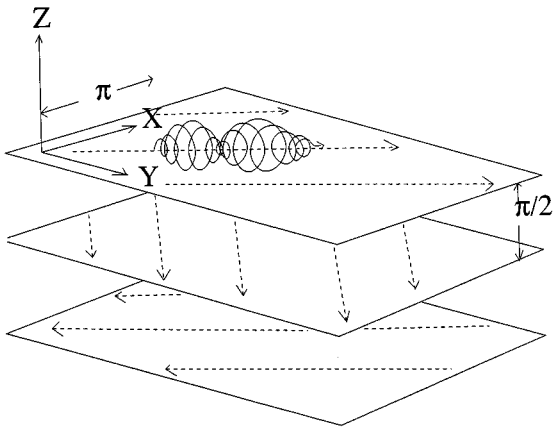


FIG. 2. Structure of the $\mathcal{A}_2$ flow, showing straight streamlines (dashed lines) on the $z=\pi/4+m\pi/2$ planes, and the converging and diverging swirl of the flow around these streamlines.

tortion of the isosurfaces of the other; however, averaging over angles we find that $\langle|\nabla\omega^2|^2\rangle=6\omega^2$, so that near the maximal point

$$|\nabla\xi|^2\approx\frac{A^2+B^2+C^2}{2\omega^2}. \tag{27}$$

Going on to curvature, its behavior is close to that of the $|\nabla\xi|$, since the curvature in these flows stems not from curving of tubes of well-aligned vortex lines but directly from the swelling and swirling inherent in the $|\nabla\xi|$ itself. The major difference is that at the points of minimal vorticity of the $\mathcal{A}_2$ flow the curvature is zero (being on the straight streamlines) and small in its neighborhood, while the $|\nabla\xi|$ is at a peak at these points due to the strong swirl of the flow around them.

Furthermore, the PDFs of curvature and $|\nabla\xi|$ can also be understood in these terms, as seen in Figs. 1(a) and 1(c). Since the curvature is zero only on isolated lines (that is, the two-dimensional measure of the set is zero) the PDF is zero at $c=0$ for both $\mathcal{A}_1$ and $\mathcal{A}_2$ flows. The dependence of the PDF on the gradient seen in Eq. (23) does not affect this conclusion, since one can verify that $\nabla c$ is nonzero at the streamlines. However, due to the dense network of straight streamlines in the $\mathcal{A}_1$ flow, the PDF peaks at very low curvatures that fill the regions close to the straight streamlines. In the $\mathcal{A}_2$ flow, with its relatively sparse $c=0$ set, the PDF peaks at a higher curvature. For this flow with its narrower range of vorticities the distribution of curvature too has a narrow range, with no high curvatures available in the $\mathcal{A}_1$ flow near the stagnation points.

On the other hand, the $\nabla|\nabla\xi|$ is extremal on the straight streamlines in both flows; one can verify that $\nabla|\nabla\xi|=0$ on these streamlines. Thus, as expected from Eq. (23), we have a cusp in the PDF at minimal $|\nabla\xi|$.

To summarize our analysis of the ABC flows, we have shown that the results of our numerical analysis of the geometry of a simple flow are reasonable and understandable in terms of the analytic form of the flow.

### C. Geometry of the Re=20 flow

We now consider the Re=20 flows. As we have said, these are divided into metastable periods of $\mathcal{A}_2$ flows, distorted by small-scale components, and transient bursts; in these bursts there is rapid change between the relative strengths of the largest (ABC) modes and heightened small-scale activity. The examination of this flow will allow us to examine the effect of small-scale flows and disorder on the geometry.

As expected, consideration of Figs. 1(a)–1(d) shows that the geometry of the metastable flow is very similar to that of the $\mathcal{A}_2$ flow. The main difference is a broadening of the distribution of $|\nabla\xi|$. The added distortion to all regions also shifts the whole distribution to higher values of the $|\nabla\xi|$. This similarity is not surprising since the metastable flow is a smooth distortion of the $\mathcal{A}_2$ flow by small-scale distortions. What is less expected is the remarkable similarity between the geometrical statistics of the small-scale bursts and of the $\mathcal{A}_1$ flow. Again, a broadening of the distribution of $|\nabla\xi|$ is the main difference between these flows.

There are two possible explanations for this similarity; both probably have a role. One is that as one near-$\mathcal{A}_2$ flow melts into another, the magnitudes of the three ABC modes approach closer to one another. This, despite strong distortion by small-scale flow, plausibly produces something not too far from the $\mathcal{A}_1$ flow, which is that flow with all modes equal in strength. Another explanation is the kinematic constraints of incompressible flow: as the distortion of the metastable flow creates regions of low vorticity, the vortex lines in these regions necessarily swell, which will enhance misalignment and curvature unless for some reason the swirl is simultaneously reduced. In dynamic language, as we can see from Eq. (12), this means that the compression (negative stretching rate $\alpha$) of the vortex lines, necessary to create weak vorticity from strong, almost inevitably enhances curvature and misalignment.

Finally, we briefly treat torsion. The torsion in the $\mathcal{A}_1$ flow is almost all of one sign, so that the flow breaks the chiral symmetry. The torsion in the $\mathcal{A}_2$ flow seems essentially symmetrical, with an equal amount of points of each sign. In both cases the torsion is high for both low and high vorticities, which seems to be a particular property of ABC flows. The small-scale and metastable Re=20 flows are again respectively similar, except for some broadening of distributions.

So what do we conclude from the Re=20 flow? First of all, as we saw in the ABC flows, the existence of sizable curvature and misalignment do not imply the existence of dominant small-scale components of the flow. In large-scale flows the curvature and misalignment must appear near vorticity neutral points. Second, in low Reynolds flows the geometrical statistics can be explained by a combination of kinematic constraints and the influence of the forcing.

### D. Re=30 flow

In the Re=30 flow the ABC modes now act chaotically, although Fig. 3 suggests that they still may be attracted to the $\mathcal{A}_1$ and the $\mathcal{A}_2$ states; the behavior around the times $t=540,635,670$ and $t=600,655$ suggests an attraction to the $\mathcal{A}_1$ and the $\mathcal{A}_2$ states, respectively. The behavior of the en-

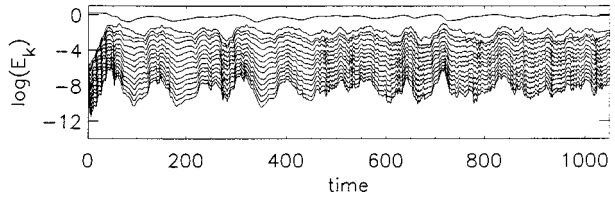


FIG. 3. Behavior with time of energies in ABC modes in Re=30 flow (for a subset of the data). Note the closeness to $\mathcal{A}_2$ flow around, e.g., $t=650$, 870, 970, and 1020 and to $\mathcal{A}_1$ flow around, e.g., $t=690$, 820, and 1040. Solid line, (1,0,0); dotted line, (0,1,0); dashed line, (0,0,1). Logarithms are to base 10.

ergies in shells in $k$ space of constant width $\Delta k=1$ is much smoother than in the Re=20 flow, with no metastable flows or bursts, as can be seen in Fig. 4. The statistics of geometry show that in this respect the Re=30 flow is closer to the small-scale bursts than to the metastable periods of the Re =20 flow. There is some broadening of the distributions of $|\nabla\xi|$ and curvature, high values in particular of both being more probable. The $|\nabla\xi|$ and curvature in regions of low vorticity magnitude are if anything even stronger. Torsion here varies little over a wide range in vorticity, except for high values in regions of low vorticity magnitude, as the specific character of ABC flow is lost.

Finally, for higher Reynolds numbers (from Re=100 and up) all residual order disappears from the behavior of the modes and the gap in magnitude between $k=1$ and smaller-scale modes disappears, making way for a continuous spectrum.

## V. DYNAMICS AND GEOMETRY

In this section we analyze the connection between vortex line geometry and vortex dynamics as seen in our simulations. We will refer mostly to the Re=2200 ABC-forced data, as most representative of strong turbulence; when we refer to other data we will mention this explicitly. The Re =2200 data are averaged over 140 data sets, each consisting of the complete flow of $192^3$ points at a certain time. This collection of data sets spans over 15 turnover times of the flow. The energy spectrum of the flow agrees with the results of previous simulations and shows good resolution of small scales.

The WDFs in Fig. 5 clearly show that for most of the range of vorticity the curvature of vortex lines goes down as the magnitude of their vorticity goes up. There seems to be some saturation at high vorticities. Assuming our discussion of Sec. II B to be comprehensive, several mechanisms could be responsible for the straightness of strong vortices. One

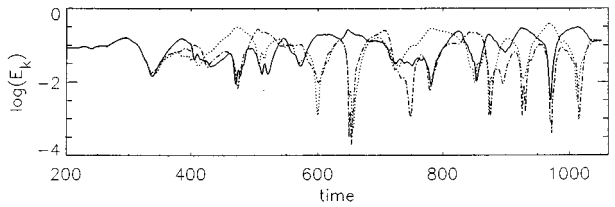


FIG. 4. Behavior of shell energies in Re=30 flow, showing a disappearance of all metastable flow. Logarithms are to base 10.

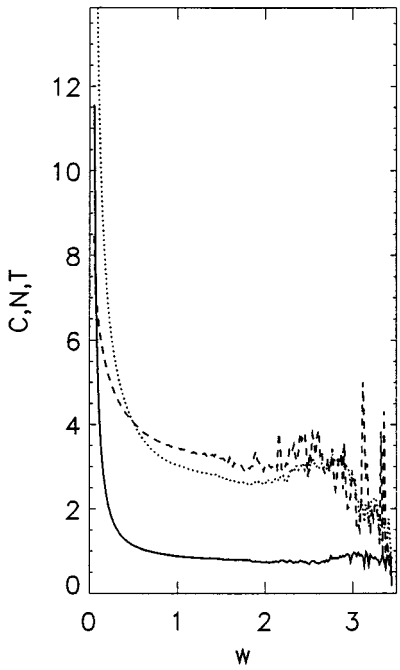


FIG. 5. WDFs of dependence on geometry. Solid line, curvature $c$; dotted line, torsion $T$; dashed line, misalignment $N$ vs vorticity. The statistics are averaged over 140 flow samples of Re=2200 flow. Note the saturation at high vorticities.

could, however, conclude that the saturation at high vorticities is due to local induction of stretching by strongly curved vortices, since no other effect seems available to cancel the tendency of vortices to straighten as their vorticity goes up.

We go on to examine one particular mechanism for straightening strong vortices, that in which stretching both enhances vorticity and straightens vortex lines. We recall that, on the other hand, the analysis of Ref. [7] showed no connection between stretching of vortices and their alignment. The WDFs of Fig. 6 show that while the inviscid vorticity growth rate $\alpha$ of Eqs. (4) and (12) goes down with curvature, this is not true of $|\alpha|$, or of $\alpha$ as a function of the misalignment. It seems reasonable to explain these findings as showing that indeed stretching straightens curved vortex lines; then if we ignore the difference between stretching and *compression* by the strain by looking at $|\alpha|$, the effect balances out and we have a slight growth of $|\alpha|$ with curvature, probably stemming from a weaker effect of local induction of $\alpha$ by curvature, as seen in Fig. 6. Any other explanation for the curvature-stretching rate correlation, such as some effect acting both on vortex line curvature and strain, must explain this sensitivity to the phase of the strain. The finding that $\alpha$ shows no particular dependence on the misalignment $N$ supports the picture in Ref. [7] of straightening, but not aligning, of vortex tubes by stretching. To better see the regions of very strong stretching we show in Fig. 7 the WDF of curvature as a function of $\alpha$. For lower $\alpha$'s the curvature goes down with $\alpha$. However, for very high $\alpha$, corresponding to the tail of the PDF of the $\alpha$ (not shown), we indeed see a tendency towards higher curvatures, so we can see here more clearly the effect of local induction. This does not appear in the $\alpha$ vs $c$ statistics of Fig. 6 at high curvatures, since many

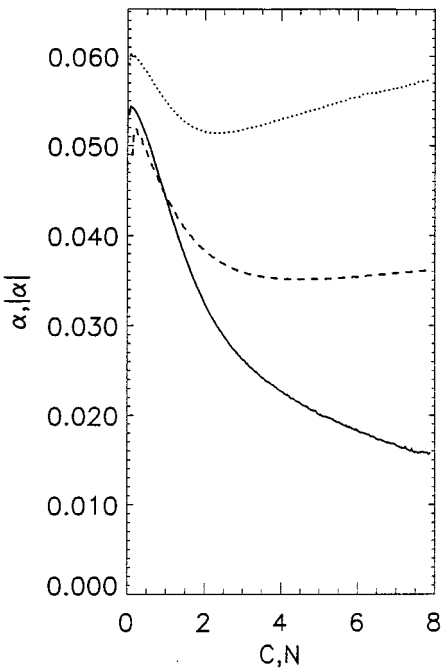


FIG. 6. Solid line, WDF of $\alpha$ vs curvature $c$; dotted line, $\alpha$ vs misalignment $N$; dashed line, $|\alpha|$ vs curvature. The statistics are averaged over 140 flow samples of Re=2200 flow.

strongly curved points are in low vorticity regions with low $\alpha$.

One might doubt the connection assumed (to a certain extent) above between $\alpha$ and the magnitude of vorticity, since the former is only an instantaneous measure of vorticity growth and no guarantee of continued growth. However,

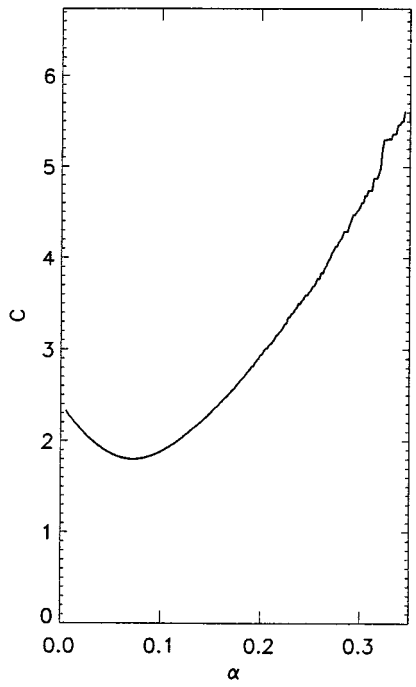


FIG. 7. WDF (dependence) of $c$ on stretching rate $\alpha$ in Re =2200 flow. The statistics averaged over 140 flow samples. Note the curved geometry at very high stretching from local effects.

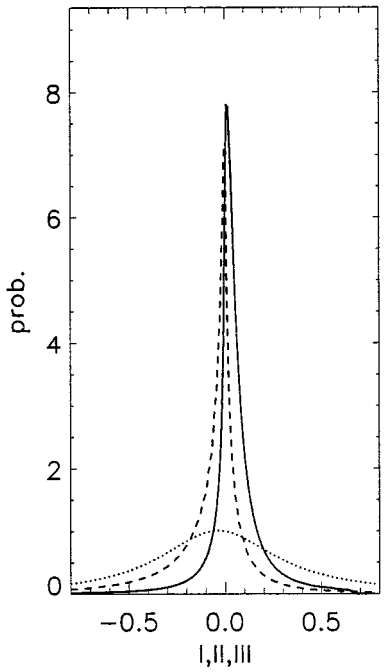


FIG. 8. Comparison of the terms in the curvature equation in terms of magnitude. Solid line, PDF of the first term in the curvature equation; dotted line, second term; dashed line, third term. The statistics are averaged over 140 flow samples of Re=2200 flow. Note particularly the large size but small average of the second term.

the WDF (not shown) of $\alpha$ vs $\omega$ shows that the correlation between the two is strong and monotonic, presumably because vorticity is built rather quickly and smoothly.

To confirm our picture of vortex dynamics we have analyzed separately the terms of Eq. (12) for the curvature. As we stated in the Introduction, the picture of vortex tubes straightening as they strengthen depends on the first (homogenous) term being dominant, at least over time, in areas of vorticity growth. In Fig. 8 we see the PDF of the three terms. The first term has a definite tendency to be positive. (This is connected with the breaking of time symmetry in turbulent flows by the energy cascade, also manifested in the positive sign of the determinant of the strain tensor and the negative third velocity difference cumulant or skewness.) The second term reaches the largest absolute values but has the smallest space-time average since positive values are balanced by negative ones. The third term has a tendency to be negative, presumably explained by the residual chiral symmetry breaking of the flow; in the simulations stirred by a random force this effect disappears.

In Fig. 9 we can see the WDF of the dependence of the sum of the second and third terms on the first, for data sets of points over various thresholds of vorticity magnitude. The first things that strikes the eye is that contrary to the naive expectation, there is a definite correlation between the magnitude of the first and other terms. We can see that for points being compressed ($\alpha<0$) the second and third terms dominate the first, weakening the connection between curvature and vorticity. For points being stretched, on the other hand ($\alpha<0$), the first term dominates, and this is increasingly marked for high values of $\alpha$ and high vorticities. This re-

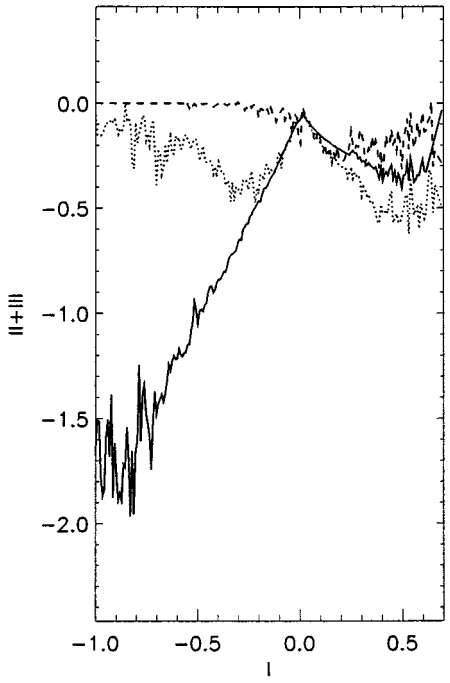


FIG. 9. WDF (dependence) of the sum of the second and third terms in the curvature equation on the first term. Solid line, threshold over $\omega_{max}/4$; dotted line, threshold over $\omega_{max}/2$; dashed line, threshold over $3\omega_{max}/4$. The statistics are averaged over 140 flow samples of Re=2200 flow. Note the increased dominance of the first term at high vorticities.

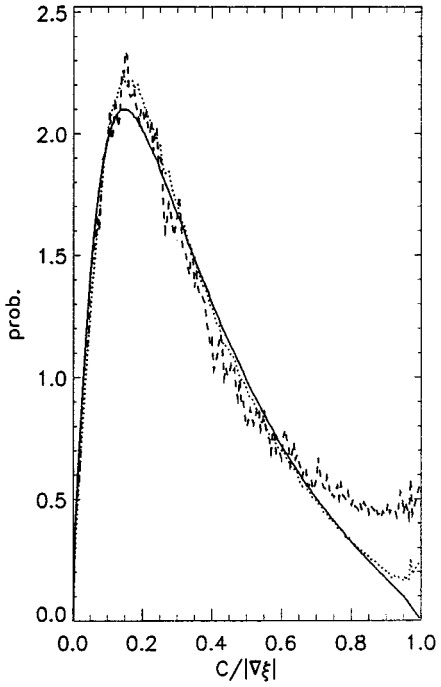


FIG. 10. PDF of $c/|\nabla\boldsymbol{\xi}|$. Solid line, threshold over $\omega_{max}/4$; dotted line, threshold over $\omega_{max}/2$; dashed line, threshold over $3\omega_{max}/4$. The statistics are averaged over 140 flow samples of Re =2200 flow.

moves the fear that hidden correlations between terms of Eq. (12) could cancel the straightening effect of stretching.

We thus conclude our discussion of the straightening of vortex lines by stretching by saying that indeed it seems that this effect is real and seems as expected to make strong vortex lines straight but not aligned. This brings us to examine the correlation between curvature and the misalignment $N$ or the total distortion $|\nabla\boldsymbol{\xi}|$. One might think from the above discussion, and assuming that straightening by stretching is the main effect determining the dependence of vorticity on geometry, that the misalignment would not go down with vorticity, since no analytic connection has been found between stretching and misalignment. In fact, as we can see from Fig. 5, at low vorticities $N$ goes down with vorticity just as strongly as curvature, if not more so; at higher vorticities we see a saturation similar to that for the curvature. Judging by the stretching effect, one would expect that in the strongest tubes curvature would be a small part of the $|\nabla\boldsymbol{\xi}|$. In fact, the plot of the ratio $c/|\nabla\boldsymbol{\xi}|$ for data sets thresholded by different vorticity magnitudes (Fig. 10) shows that the dependence on vorticity magnitude is weak and that at the highest vorticities the probability of curvature-dominated tubes become *higher*. Pictorially this means that curved tubes of well-aligned vortex lines are common in high vorticity regions; this is indeed observed in simulated flow fields. The PDFs of the ratio $c/|\nabla\boldsymbol{\xi}|$ for various Reynolds numbers seen in Fig. 11 show that the distribution of this ratio, including that fact the curvature is not usually the dominant component of the $|\nabla\boldsymbol{\xi}|$, is very robust. All this would imply that at least for some vorticities the effect of the stretching mechanism is not the dominant one compared to the other effects mentioned in Sec. II B. Comparisons of these distributions to the results of lower Reynolds runs and to runs forced by a random forcing show that all conclusions are in no way affected.

To conclude this survey of our results we turn to torsion, which is treated only briefly in this study. The analysis of Sec. II B would suggest that torsion will go down with vorticity, but much less strongly than curvature or misalignment, and this expectation is borne out as can be seen in Fig. 5, where the dependence of torsion on vorticity is shown. Saturation, even higher torsion, for high vorticities is again seen, again presumably due to local induction of stretching: besides, e.g., curvature, torsion too contributes locally to the growth rate, and one can derive terms proportional to the torsion in an expansion around $\mathbf{x}$ of $\alpha(\mathbf{x})$. This could create a tendency of $\alpha(\mathbf{x})$ and thus the local vorticity to go up with torsion and explain the saturation.

In Fig. 12 we can see the dependence of the curvature, $|\nabla\boldsymbol{\xi}|$, and torsion on the Taylor scale Reynolds number. We have made a log-log plot of each quantity normalized by the integral scale $L$, in order to compare them to various length scales that act like $L\mathrm{Re}^{-\chi}$ for high Reynolds number. The $L$'s used were the average over the calculated $L$ for each run, which differ slightly from run to run (see Table I). In order to compare better with scaling behavior, we have also plotted the pointwise slopes from the log-log plots.

Although one cannot speak of a real power law behavior in such a narrow range of Reynolds numbers, the curvature and $|\nabla\boldsymbol{\xi}|$ at least seem to be quite close to a power-law, and furthermore to the same power law, within the variations seen. The pointwise exponents are not constant and have averages of $\chi=1.0$ for curvature and $|\nabla\boldsymbol{\xi}|$ and $\chi=0.85$ for torsion, the latter number being rather unreliable. Our result

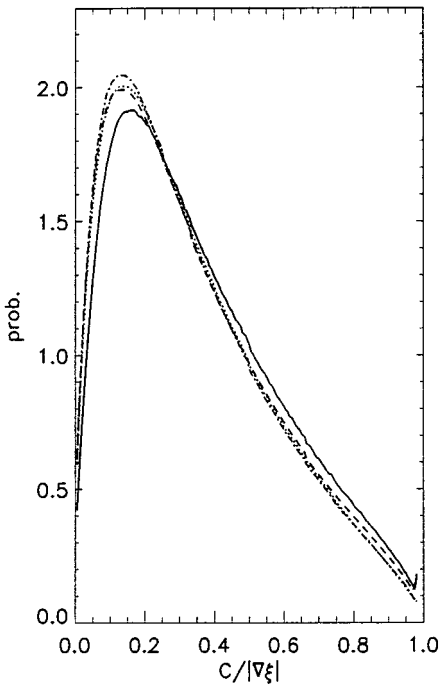


FIG. 11. PDF of $c/|\nabla\boldsymbol{\xi}|$ in runs with Re=100 (solid line), Re =1000 (dotted line), Re=1500 (dot-dashed line), and Re=2200 (dashed line). Statistics averaged over 40, 40, 20, and 140 flow samples, respectively. Note the robustness of the result.

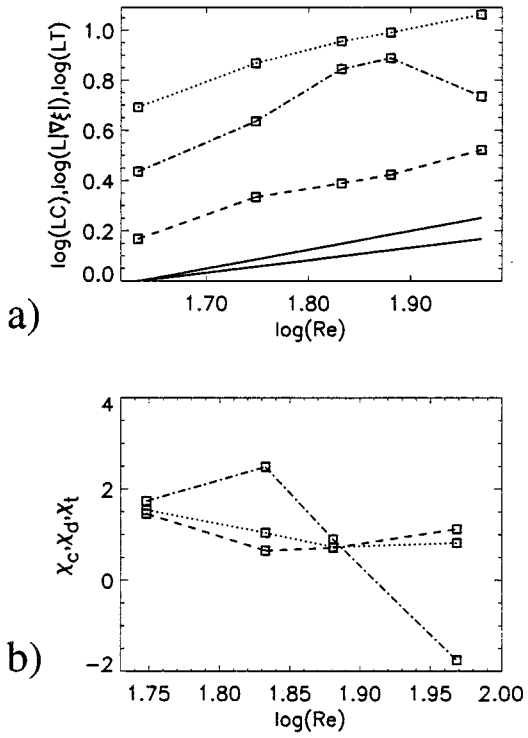


FIG. 12. (a) Average curvature, $|\nabla\boldsymbol{\xi}|$ and torsion vs average Taylor scale Re in the ABC-forced runs. The quantities are normalized with the average integral scale $L$ as measured in each run. (b) Scaling exponents of curvature $|\nabla\boldsymbol{\xi}|$ and torsion (e.g., $c\sim \mathrm{Re}^{\chi_c}$) estimated from the pointwise slopes in graph (a). The statistics are averaged over 40, 40, 20, and 140 flow samples, respectively. All logarithms are to base 10.

cannot rule out a scaling with the Kolmogorov length $L^{-1}\mathrm{Re}_\lambda^{3/4}$; given the limited range one would hesitate to rule out even the Taylor length scaling $L^{-1}\mathrm{Re}_\lambda^{1/2}$. However, the possibility of a ''deep-dissipation ''scale scaling as $L\mathrm{Re}_\lambda^{-1}$ is intriguing and hints of new physics below the dissipation scale.

We finally compare briefly with the case of magnetohydrodynamic flux tubes. Since the equation for the magnetic field in magnetohydrodynamics is formally identical to that of vorticity in NS dynamics, the first three effects mentioned in Sec. II B, creating a negative correlation between curvature and $|\nabla\boldsymbol{\xi}|$ on vorticity magnitude should hold for the connection between the flux line curvature and $|\nabla\boldsymbol{\xi}|$ and magnetic field. An initial numerical analysis of this connection was presented in Ref. [20], where the curvature and $|\nabla\boldsymbol{\xi}|$ of flux lines were calculated in a direct numerical magnetohydrodynamic simulation for point sets thresholded by various magnetic-field magnitudes. The result was that curvature and $|\nabla\boldsymbol{\xi}|$ went down consistently with magnetic field. This supports our general picture, although the results of Ref. [20] do not allow an exact comparison. One should note that since in flux tubes locally induced growth (the fourth effect of Sec. II B) does not exist, the dependence of flux tube geometry on magnetic field is simpler than the dependence of vortex line geometry on vorticity.

## VI. CONCLUSION

As this article appears to be first in offering a detailed study of the geometry of vortex lines in turbulent flows, it is noteworthy that such an analysis seems to be possible and meaningful. The answers we got are reasonable and self-consistent. Different runs yield robust results that do not depend on minute details. The main physical conclusions that can be drawn from our simulations are as follows.

(i) Vortex lines in regions of strong vorticity tend to be well aligned and straight (see Fig. 5). Alignment gets better the higher the vorticity, although at the highest values of the vorticity we observed a saturation in the decline of the alignment.

(ii) As proposed in [7], the stretching of vorticity indeed tends to straighten vortex lines. Numerically this is seen as the appearance of strong correlations between the stretching and the straightness of the vortex lines (see Fig. 6). The main potential pitfall in this expectation, the potentially canceling effect of additional terms, was shown to be unfounded (see Fig. 9).

(iii) It is not obvious that the mechanism verified in (ii). is the dominant cause for the phenomenon found in (i). For one thing, there is no theoretical expectation of a connection between alignment and stretching, but as we show the increase in alignment with vorticity is just as strong as the increase in straightness. It is possible that the stretching mechanism is responsible for straightening and that there exists another, yet unidentified, mechanism for alignment. It is also possible that the effect of kinematic constraints in lower vorticities and of viscid diffusion in higher vorticities, acting both on curvature and misalignment, greatly dominates in size the stretching effect.

Needless to say, the curbing of finite-time singularities

necessitates both straightness *and* alignment. Thus the alignment at high vorticities seen in our simulations supports the general idea that there may exist a self-correcting mechanism that explains the rarity of such singular behavior in simulations of the incompressible Navier-Stokes equations. Although we do not have a full dynamical theory of the increased alignment, its observation strengthens the connection between vortex dynamics and regularity.

## ACKNOWLEDGMENTS

This work has been supported in part by the U.S.–Israel Binational Science Foundation. We thank Peter Constantin and Axel Brandenburg for important discussions. B.G. acknowledges the German-Israeli Foundation and Naftali and Anna Backenroth-Bronicki Fund for Research in Chaos and Complexity.

## APPENDIX: EQUATIONS FOR NUMERICAL CALCULATION OF GEOMETRICAL QUANTITIES

Direct calculation of curvature, $|\nabla\boldsymbol{\xi}|$, and torsion is problematic since their calculation involves differentiating the direction field $\boldsymbol{\xi}$, which is nonanalytic at points where $\boldsymbol{\omega}=0$. In particular differentiation of the $\boldsymbol{\xi}$ field cannot be performed in Fourier space.

Thus for purposes of calculation we used formulas that involved only derivatives of the vorticity field itself. We first define (and in calculations calculate)

$$A\equiv(\boldsymbol{\omega}\cdot\nabla)\omega^2, \tag{A1}$$

$$\mathbf{B}=\boldsymbol{\omega}\times\mathbf{c}, \tag{A2}$$

and

$$\mathbf{E}=(\boldsymbol{\omega}\cdot\nabla)\boldsymbol{\omega}. \tag{A3}$$

From the definition of the curvature vector $\mathbf{c}=(\boldsymbol{\xi}\cdot\nabla)\boldsymbol{\xi}$ we can easily find that

$$\mathbf{c}=\frac{1}{\omega^2}\left[\mathbf{E}-\frac{1}{2\omega^2}A\boldsymbol{\omega}\right] \tag{A4}$$

and the curvature is $c=|\mathbf{c}|$.

The torsion is defined as $T=\mathbf{b}\cdot(\boldsymbol{\xi}\cdot\nabla)\mathbf{n}$. Using $\mathbf{b}=\boldsymbol{\xi}\times\mathbf{n}$ we can write

$$T=-\frac{1}{\omega^2c^2}\mathbf{B}\cdot(\boldsymbol{\omega}\cdot\nabla)\mathbf{c}. \tag{A5}$$

Using the equation above for $\mathbf{c}$ we can write

$$(\boldsymbol{\omega}\cdot\nabla)\mathbf{c}=-\frac{3A}{2\omega^4}\mathbf{E}+\frac{1}{\omega^2}(\boldsymbol{\omega}\cdot\nabla)(\boldsymbol{\omega}\cdot\nabla)\boldsymbol{\omega} \tag{A6}$$

$$+\frac{2}{\omega^6}A^2\boldsymbol{\omega}-\frac{1}{2}\frac{\boldsymbol{\omega}}{\omega^4}(\boldsymbol{\omega}\cdot\nabla)(\boldsymbol{\omega}\cdot\nabla)\omega^2. \tag{A7}$$

We then find that

$$(\boldsymbol{\omega}\cdot\nabla)(\boldsymbol{\omega}\cdot\nabla)\boldsymbol{\omega}=(\mathbf{E}\cdot\nabla)\boldsymbol{\omega}+\sum_{i,j}\omega_i\omega_j\partial_i\partial_j\boldsymbol{\omega}. \tag{A8}$$

Since we are multiplying $(\boldsymbol{\omega}\cdot\nabla)\mathbf{c}$ by $\mathbf{B}=\boldsymbol{\omega}\times\mathbf{c}$, we can set all terms in $(\boldsymbol{\omega}\cdot\nabla)\mathbf{c}$ that are proportional to $\boldsymbol{\omega}$ or $\mathbf{c}$ to zero and have

$$T=\frac{1}{\omega^2}\mathbf{B}\cdot\left[\frac{3}{\omega^2}A\mathbf{E}-(\mathbf{E}\cdot\nabla)\boldsymbol{\omega}-\sum_{i,j}\omega_i\omega_j\partial_i\partial_j\boldsymbol{\omega}\right]. \tag{A9}$$

Finally, the $|\nabla\boldsymbol{\xi}|$ is calculated through

$$|\nabla\boldsymbol{\xi}|^2=\left|\nabla\left(\frac{\boldsymbol{\omega}}{\omega}\right)\right|^2=\frac{1}{\omega^6}\sum_{i,j}\left(\omega^2\partial_j\omega_i-\frac{1}{2}\omega_i\partial_j\omega^2\right)^2. \tag{A10}$$

[1] A. Vincent and M. Meneguzzi, J. Fluid Mech. **225**, 1 (1991).
[2] S. Chen and X. Shan, Comput. Phys. **6**, 643 (1992).
[3] M. Tanaka and S. Kida, Phys. Fluids A **5**, 2079 (1993).
[4] J. Jiménez, A.A. Wray, P.G Saffman, and R.S. Rogallo, J. Fluid Mech. **255**, 65 (1993).
[5] E.J. Hopfinger, F.K. Browand, and Y. Gagne, J. Fluid Mech. **125**, 505 (1982).
[6] S. Douady, Y. Couder, and M.E. Brachet, Phys. Rev. Lett. **67**, 983 (1991).
[7] P. Constantin, I. Procaccia, and D. Segel, Phys. Rev. E **51**, 3207 (1995).
[8] P. Constantin and Ch. Fefferman, Indiana Univ. Math. J. **42**, 775 (1993).
[9] R.M. Kerr, Phys. Fluids A **5**, 1725 (1993).
[10] O.N. Boratav and R.B. Pelz, Phys. Fluids **7**, 1712 (1995).
[11] S.B. Pope, P.K. Yeung, and S.S. Girimaji, Phys. Fluids A **1**, 2010 (1989); S.S. Girimaji, *ibid.* **3**, 1772 (1991).
[12] I.T. Drummond and W. Munch, J. Fluid Mech. **225**, 529 (1991); I.T. Drummond, *ibid.* **252**, 479 (1993).
[13] M. Liu and F.J. Muzzio, Phys. Fluids A **8**, 75 (1996).
[14] W. Klingenberg, *A Course in Differential Geometry* (Springer, Berlin, 1978).
[15] V.I. Arnold, C. R. Acad. Sci. (Paris) **261**, 17 (1965).
[16] D.J. Galloway and U. Frisch, J. Fluid Mech. **180**, 557 (1987).
[17] O. Podvigina and A. Pouquet, Physica D **75**, 471 (1994).
[18] S. Childress and A.M. Soward, in *Chaos in Astrophysics*, edited by J.R. Buchler, J.M. Perdang, and E.A. Spiegel (Reidel, Dordrecht, 1985). Note that Childress and Soward's coordinates are different from ours by $x_i=\pi/2-x_i$.
[19] T. Dombre, U. Frisch, J.M. Greene, M. Henon, A. Mehr, and A.M. Soward, J. Fluid Mech. **167**, 353 (1986).
[20] A. Brandenburg, I. Procaccia, and D. Segel, Phys. Plasmas **2**, 1148 (1995).